THE JOURNAL OF CHEMICAL PHYSICS **122**, 014312 (2005)

A full-dimensional quantum dynamical approach to the vibrational predissociation of Cl_2-He_2

A. García-Vela[a)]
Instituto de Matemáticas y Física Fundamental, CSIC, Serrano 123, 28006 Madrid, Spain

(Received 19 May 2004; accepted 11 October 2004; published online 15 December 2004)

A full-dimensional, fully coupled wave packet method is proposed and applied to investigate the vibrational predissociation dynamics of the $Cl_2(B,v')-He_2$ complex. Simulations are carried out for the resonance states associated with the $v'=10-13$ initial vibrational excitations of Cl_2, and the results are compared with the available experimental data. A good agreement with experiment is achieved for the resonance lifetimes (typically within experimental error) and the Cl_2 fragment rotational distributions. The mechanism of dissociation of the two He atoms is found to be dominantly sequential, through the $\Delta v'=-2$ channel. The probabilities obtained for the $\Delta v'=-1$ dissociation channel are, however, overestimated due to the use of absorbing boundary conditions combined with finite grid effects. It is suggested that a mechanism of energy redistribution through the couplings between the van der Waals modes of the two weak bonds takes place in the $\Delta v'=-1$ dissociation. This mechanism is consistent with the resonance lifetimes and Cl_2 rotational distributions predicted. The favorable comparison with most of the experimental data supports the reliability of the potential used to model $Cl_2(B,v')-He_2$, at least in the present range of v' levels. © *2005 American Institute of Physics.* [DOI: 10.1063/1.1827600]

I. INTRODUCTION

The study of weak van der Waals (vdW) interactions between chemical species and rare gas atoms has attracted much interest in the last two decades. Such interactions play a central role in determining the physical and chemical properties of doped clusters and condensed matter environments. Triatomic complexes such as BC–Rg, with a BC diatomic molecule weakly bound to a Rg rare gas atom, are among the simplest prototypical systems where the vdW interaction is present. The spectroscopy and photodissociation dynamics of complexes such as Cl_2-Rg,[1–3] Br_2-Rg,[4–8] I_2-Rg,[9–14] and ICl–Rg (Refs. 15–17) (Rg=He,Ne,Ar) have been investigated experimentally. Quantum mechanical simulations of the spectroscopic and dynamical properties measured are currently performed, with an accuracy limited essentially only by the accuracy of the potential surface used.[6,18–22] A number of experiments on $BC-Rg_n$ complexes with $n\geqslant 2$ have been reported as well.[3,9,10,23–27] However, a full-dimensional quantum-dynamical treatment of these systems, even for the smallest $n=2$ size, is still a challenge to theory.

A variety of approximate dynamical treatments has been applied to study $BC-Rg_n$ complexes. Classical and quasiclassical simulations of the vibrational predissociation (VP) dynamics of clusters such as I_2-He_n $(n=1-9)$,[28] I_2-Ne_n $(n=1-9)$,[29,30] and I_2-Ar_{13},[31] have been carried out. Hybrid classical-quantum and quantum-classical methods have been applied to investigate the predissociation dynamics of Cl_2-He_2,[32] I_2-Ne_n $(n=2-6)$,[33] and Cl_2-Ne_n $(n=2,3)$.[34] Quantum-dynamical simulations on $BC-Rg_2$ complexes were performed using reduced-dimensional models including three[35,36] and four[37,38] degrees of freedom. A full-dimensional quantum method based on a decoupling scheme of some of the modes was applied to simulate the VP of Cl_2-Ne_2 and I_2-Ne_2.[39] In general, the above approximate methods have shown reasonable success in describing some of the properties measured experimentally, while those properties which are more directly affected by the approximations involved are more poorly reproduced. Recently, an exact full-dimensional quantum dynamical treatment of the I_2-Ne_2 predissociation using the multiconfiguration time-dependent Hartree (MCTDH) method has been reported,[40] although no comparison with experiment was made.

The obvious advantage of approximate methods is their computational efficiency. However, when quantum effects (mostly neglected in quasiclassical and hybrid quantum-classical approaches) and spatial delocalization and intermode couplings (not well described in reduced-dimensional quantum models) become important, approximate methods may be inadequate. This is the case of the Cl_2-He_2 complex, where the He atoms are highly quantal objects and the spatial delocalization of the system is important. Thus, in order to be reasonably quantitative in the description of the Cl_2-He_2 dynamics, an exact quantum-mechanical treatment would be required.

In this paper the vibrational predissociation of Cl_2-He_2 is investigated through an exact full-dimensional quantum method. The goal of the present work is twofold. The first objective is to develop a quantum-mechanical methodology which allows one to describe realistically the experimental data available for this system.[26,41] The second goal is to test the accuracy of the potential-energy surface used to model the complex. Recently an empirical potential surface for the

[a)]Electronic mail: garciavela@imaff.cfmac.csic.es

$Cl_2(B)-He$ triatomic complex has been proposed,[22] which reproduces well the available spectroscopic and dynamical experimental data. Using this surface to model the $Cl_2(B)-He_2$ potential can provide a valuable additional test on the reliability of the $Cl_2(B)-He$ potential surface previously proposed.

The paper is organized in the following way: In Sec. II the $Cl_2(B)-He_2$ potential-energy surface and the dynamical method are described. The results are presented and discussed in Sec. III. Finally, some conclusions are drawn in Sec. IV.

II. METHODOLOGY

A. Potential-energy surface

The VP process in the Cl_2-He_2 complex occurs upon optical excitation of the Cl_2 chromophore from the ground electronic state to a vibrational state $v'>0$ in the B excited electronic state. A resonance state $Cl_2^*(B,v')-He_2$ is prepared in this way, which decays to a dissociation continuum, leading to fragmentation of the complex into $Cl_2(B,v_f<v')+He+He$. Such a fragmentation is caused by energy transfer from the Cl_2 stretching vibration to the vdW modes.

The Cl_2-Ne_2 system is represented in bond coordinates $\mathbf{r}$, $\mathbf{R}_1$, and $\mathbf{R}_2$, where $\mathbf{r}$ is the vector associated with the Cl–Cl bond, and $\mathbf{R}_1$ and $\mathbf{R}_2$ are the vectors joining the Cl_2 center of mass and the He atoms, respectively. In this representation, by expressing the above vectors in spherical coordinates [$\mathbf{r}=(r,\theta_r,\phi_r)$, $\mathbf{R}_i=(R_i,\theta_i,\phi_i)$, $i=1,2$] the Hamiltonian of the system becomes

$$\hat{H}=-\frac{\hbar^2}{2\mu_{Cl_2}}\frac{\partial^2}{\partial r^2}+\frac{\mathbf{j}^2}{2\mu_{Cl_2}r^2}-\frac{\hbar^2}{2\mu_{Cl_2-He}}\left(\frac{\partial^2}{\partial R_1^2}+\frac{\partial^2}{\partial R_2^2}\right)+\frac{1}{2\mu_{Cl_2-He}}\left(\frac{\mathbf{l}_1^2}{R_1^2}+\frac{\mathbf{l}_2^2}{R_2^2}\right)-\frac{\hbar^2\boldsymbol{\nabla}_1\cdot\boldsymbol{\nabla}_2}{2m_{Cl}}+V(\mathbf{r},\mathbf{R}_1,\mathbf{R}_2), \tag{1}$$

where $\mu_{Cl_2}=m_{Cl}/2$ and $\mu_{Cl_2-He}=m_{He}2m_{Cl}/(m_{He}+2m_{Cl})$ are the reduced masses corresponding to the Cl_2 and vdW modes, respectively, with $m_{Cl}=35.4527$ amu and $m_{He}=4.0026$ amu, $\mathbf{j}$, $\mathbf{l}_1$, and $\mathbf{l}_2$ are the angular momentum operators associated with $\mathbf{r}$, $\mathbf{R}_1$, and $\mathbf{R}_2$, respectively (the total angular momentum of the system is $\mathbf{J}=\mathbf{j}+\mathbf{l}_1+\mathbf{l}_2$), and

$$\begin{aligned}\boldsymbol{\nabla}_1\cdot\boldsymbol{\nabla}_2=&(\sin\theta_1\sin\theta_2\cos\phi+\cos\theta_1\cos\theta_2)\frac{\partial^2}{\partial R_1\partial R_2}+\frac{\cos\theta_1\cos\theta_2\cos\phi+\sin\theta_1\sin\theta_2}{R_1R_2}\frac{\partial^2}{\partial\theta_1\partial\theta_2}\\&+\frac{\cos\phi}{R_1R_2\sin\theta_1\sin\theta_2}\frac{\partial^2}{\partial\phi_1\partial\phi_2}+\frac{\sin\theta_1\cos\theta_2\cos\phi-\cos\theta_1\sin\theta_2}{R_2}\frac{\partial^2}{\partial R_1\partial\theta_2}\\&+\frac{\cos\theta_1\sin\theta_2\cos\phi-\sin\theta_1\cos\theta_2}{R_1}\frac{\partial^2}{\partial R_2\partial\theta_1}-\frac{\sin\theta_1\sin\phi}{R_2\sin\theta_2}\frac{\partial^2}{\partial R_1\partial\phi_2}-\frac{\sin\theta_2\sin\phi}{R_1\sin\theta_1}\frac{\partial^2}{\partial R_2\partial\phi_1}\\&-\frac{\cos\theta_1\sin\phi}{R_1R_2\sin\theta_2}\frac{\partial^2}{\partial\theta_1\partial\phi_2}-\frac{\cos\theta_2\sin\phi}{R_1R_2\sin\theta_1}\frac{\partial^2}{\partial\theta_2\partial\phi_1},\end{aligned} \tag{2}$$

being $\phi=\phi_1-\phi_2$. The last term of Eq. (1) comprises all the potential interactions of Cl_2-He_2. Zero total angular momentum ($J=0$) is assumed for the system.

To a good approximation, the VP process can be assumed to take place on a single potential-energy surface, namely that of the B electronic state. This potential surface is modeled as

$$\begin{aligned}V(r,R_1,R_2,\theta_1,\theta_2,\phi)&=V_{Cl_2}(r)+V_{Cl_2-He}(r,R_1,\theta_1)+V_{Cl_2-He}(r,R_2,\theta_2)\\&\quad+V_{He-He}(R_1,R_2,\theta_1,\theta_2,\phi).\end{aligned} \tag{3}$$

The diatomic potential $V_{Cl_2}(r)$ is represented by a Morse function whose parameters were given in Ref. 36. The triatomic potential $V_{Cl_2-He}(r,R_i,\theta_i)$ ($i=1,2$) has been described in detail in Ref. 22. In brief, this potential is a sum of two Morse functions, each of them describing the Cl–He interaction. Two of the three Morse parameters depend on the Cl–Cl bond distance r, which introduces a three-body character in the V_{Cl_2-He} potential surface. Finally, the He–He interaction is represented by the Tang and Toennies potential recently reported,[42] using two Born–Mayer parameters and three dispersion coefficients.

B. Resonance energies and initial state

The initial state of Cl_2-He_2 prepared by excitation needs to be specified before simulating the VP dynamics of the complex. Such a state corresponds with the ground resonance state of the system associated to the specific Cl_2 vibrational level v' excited in the B electronic state. This initial state is calculated by applying the variational formalism of Villarreal, Roncero, and Delgado-Barrio,[43] where the Hamiltonian of Eq. (1) is represented in a basis set and diagonalized. Such a basis set is defined in a body-fixed (BF) frame (in which the z axis coincides with the direction of the $\mathbf{r}$ vector). By taking into account the symmetry properties of the Cl_2-He_2 Hamiltonian, i.e., that the Hamiltonian is in-

variant under exchange of $\mathbf{R}_1$ and $\mathbf{R}_2$, the size of the basis set can be conveniently reduced. The symmetry-adapted basis functions,

$$\Xi^{J,M}_{l_1,l_2,L,\Omega,v,m,n}(\mathbf{r},\mathbf{R}_1,\mathbf{R}_2) = \left[\frac{1}{2(1+\delta_{mn}\delta_{l_1 l_2})}\right]^{1/2} [\Phi^{J,M}_{l_1,l_2,L,\Omega,v,m,n}(\mathbf{r},\mathbf{R}_1,\mathbf{R}_2) + \Phi^{J,M}_{l_2,l_1,L,\Omega,v,n,m}(\mathbf{r},\mathbf{R}_1,\mathbf{R}_2)] \quad (4)$$

are used, where

$$\Phi^{J,M}_{l_1,l_2,L,\Omega,v,m,n}(\mathbf{r},\mathbf{R}_1,\mathbf{R}_2) = \phi_{v,m,n}(r,R_1,R_2)\mathcal{W}^{J,M}_{l_1,l_2,L,\Omega}(\theta_1,\theta_2,\phi_1,\phi_2), \quad (5)$$

and similarly for $\Phi^{J,M}_{l_2,l_1,L,\Omega,v,n,m}$. The radial function $\phi_{v,m,n}(r,R_1,R_2)$ is defined as

$$\phi_{v,m,n}(r,R_1,R_2) = \chi_v(r)\xi_m(R_1)\xi_n(R_2)/rR_1R_2, \quad (6)$$

where $\chi_v(r)$ is an eigenfunction of the Cl_2 stretching mode, obtained by solving

$$\left[-\frac{\hbar^2}{2\mu_{Cl_2}}\frac{\partial^2}{\partial r^2} + V_{Cl_2}(r)\right]\chi_v(r) = E_v\chi_v(r), \quad (7)$$

and $\xi_m(R_1)$ and $\xi_n(R_2)$ are vibrational basis functions for the R_1 and R_2 coordinates.[43]

The angular functions are defined as

$$\mathcal{W}^{J,M}_{l_1,l_2,L,\Omega}(\theta_1,\theta_2,\phi_1,\phi_2) = \left(\frac{2J+1}{4\pi}\right)^{1/2} D^{J*}_{M,\Omega}(\phi_r,\theta_r,0)\mathcal{Y}^{L,\Omega}_{l_1,l_2}(\theta_1,\theta_2,\phi_1,\phi_2), \quad (8)$$

where $D^{J*}_{M,\Omega}$ are Wigner rotation matrices[44,45] relating the space-fixed (SF) and BF frames corresponding to a total angular momentum J with projections M and Ω on the Z_{SF} and Z_{BF} axes, respectively. The functions $\mathcal{Y}^{L,\Omega}_{l_1,l_2}(\theta_1,\theta_2,\phi_1,\phi_2)$ are

$$\mathcal{Y}^{L,\Omega}_{l_1,l_2}(\theta_1,\theta_2,\phi_1,\phi_2) = (-1)^{L+\Omega}(2L+1)^{1/2}\sum_{\omega}\begin{pmatrix} l_1 & l_2 & L \\ -\omega & \omega-\Omega & \omega\end{pmatrix} \times Y^{\omega}_{l_1}(\theta_1,\phi_1)Y^{\Omega-\omega}_{l_2}(\theta_2,\phi_2), \quad (9)$$

where $L=l_1+l_2$, $(\cdots)$ denotes $3-j$ symbols, and $Y^{\omega}_{l_i}(\theta_i,\phi_i)$ are spherical harmonics. Since we shall deal with $J=0$ states of Cl_2-He_2, this implies that $M=\Omega=0$, and $\mathbf{L}=-\mathbf{j}$. Detailed expressions of the Hamiltonian matrix elements in the above basis functions are given in Ref. 43.

In the basis set only one $\chi_v(r)$ state was included, namely that corresponding to the vibrational state $v=v'$ to which the Cl_2 subunit is excited in the complex. Due to the difference of frequencies the Cl_2 vibration is well separated from the vdW modes, and only one $\chi_v(r)$ state suffices, to a good approximation, for the calculation of the ground and low excited resonance states of Cl_2-He_2. The other parameters of the basis set were $l_1^{max}=l_2^{max}=L^{max}=12$ and $m^{max}=n^{max}=4$, leading to 2716 basis functions. The ground and first three excited resonance energies of $Cl_2(B,v')-He_2$ are listed in Table I for the different vibrational states v' studied ($v'=10-13$). The vibrational energies of $Cl_2(B,v')$, $E_{v'}$, are also given in the table, along with the ground resonance energies of $Cl_2(B,v')-He$, for comparison.

TABLE I. Calculated resonance energies of $Cl_2(B)-He_2$ relative to the initial Cl_2 vibrational energy level $E_{v'}$. $E_{v'}=0$ corresponds to separated Cl atoms. The ground (E_0) and first three excited resonance energies are listed, along with the ground resonance energy of $Cl_2(B)-He$ (E_0^{tri}) for comparison.

(cm^{-1})	$v'=10$	$v'=11$	$v'=12$	$v'=13$
$E_{v'}$	−1023.3	−881.8	−750.8	−630.3
E_0	−22.33	−22.20	−22.05	−21.88
E_1	−21.18	−21.05	−20.90	−20.72
E_2	−18.08	−17.95	−17.80	−17.62
E_3	−16.48	−16.38	−16.27	−16.14
E_0^{tri}	−11.23	−11.17	−11.10	−11.02

The ground resonance energy of $Cl_2(B,v')-He_2$ is very close to twice the ground energy of the triatomic $Cl_2(B,v')-He$ complex, E_0^{tri}. This is in agreement with the spectral shifts found experimentally for Cl_2-He_2, which are twice those of Cl_2-He.[41] This result was expected due to the weak He–He interaction, and the fact that the dissociation energy of the He_2 dimer is close to zero. The present E_0 energies of $Cl_2(B,v')-He_2$ ($\sim -22\ cm^{-1}$) are about $3\ cm^{-1}$ higher than the $Cl_2(B,v'=8)-He_2$ ground resonance energy found in Ref. 41 ($-25.6\ cm^{-1}$) using a different potential surface for the complex. It was shown[22] that the E_0^{tri} energies computed with the present $Cl_2(B)-He$ interaction potential reproduce the measured spectral blueshifts within experimental error (typically with a deviation of $\sim 1\%$). Thus, taking into account that E_0 is practically $2E_0^{tri}$, the $Cl_2(B,v')-He_2$ ground resonance energies of Table I are expected to be the most accurate ones reported so far. As seen from Table I, the energy of only one vibrational quantum, $E_{v'}-E_{v'-1}$, is enough to dissociate the two He atoms.

C. Dynamical simulations

The VP dynamics of $Cl_2(B,v')-He_2$ is simulated by solving the time-dependent Schrödinger equation

$$i\hbar\frac{\partial\psi(r,R_1,R_2,\theta_1,\theta_2,\phi,t)}{\partial t} = \hat{H}\psi(r,R_1,R_2,\theta_1,\theta_2,\phi,t). \quad (10)$$

Solution of this equation for a six-dimensional, fully coupled wave packet, in the case of a slow predissociation process is a computationally very demanding problem. Therefore a careful choice of the wave packet representation is needed in order to optimize the computational requirements (in memory and time). For the reactive coordinates R_1 and R_2 a grid representation is usually convenient. For nonreactive coordinates a basis set representation is typically more efficient when the number of basis functions is not too high. The

spatial delocalization of Cl_2-He_2 implies that the system is relatively localized in momentum space. This suggests that the angular coordinates can be conveniently represented by basis functions indexed to the angular momentum values, such as those defined in Eq. (8).

Thus the Cl_2-He_2 wave packet is represented by the following expansion:

$$\psi(r,R_1,R_2,\theta_1,\theta_2,\phi,t) = \sum_{v,l_1,l_2,j}\left[\frac{1}{2(1+\delta_{l_1l_2})}\right]^{1/2}[C_{v,l_1,l_2,j}(R_1,R_2,t)\mathcal{W}_{l_1,l_2,j} \times(\theta_1,\theta_2,\phi)+C_{v,l_2,l_1,j}(R_1,R_2,t)\mathcal{W}_{l_2,l_1,j} \times(\theta_1,\theta_2,\phi)]\chi_v(r)e^{-iE_vt/\hbar} \quad (11)$$

with the angular functions being those of Eq. (8), where the indices $J=M=\Omega=0$ have been dropped, and $L=j$, $\phi=\phi_1-\phi_2$. The above expression of the wave packet satisfies the symmetry properties of Cl_2-He_2, among them that the two He atoms (and therefore the two vdW bonds) are indistinguishable. Indeed, by exchanging the $\mathbf{R}_1$ and $\mathbf{R}_2$ coordinates through the permutation operator $\mathcal{P}_{12}$,

$$\mathcal{P}_{12}[C_{v,l_1,l_2,j}(R_1,R_2,t)\mathcal{W}_{l_1,l_2,j}(\theta_1,\theta_2,\phi)] = C_{v,l_1,l_2,j}(R_2,R_1,t)\mathcal{W}_{l_1,l_2,j}(\theta_2,\theta_1,-\phi) = C_{v,l_2,l_1,j}(R_1,R_2,t)\mathcal{W}_{l_2,l_1,j}(\theta_1,\theta_2,\phi), \quad (12)$$

since

$$C_{v,l_2,l_1,j}(R_1,R_2,t)=C_{v,l_1,l_2,j}(R_2,R_1,t) \quad (13)$$

and[43]

$$\mathcal{W}_{l_1,l_2,j}(\theta_2,\theta_1,-\phi)=(-1)^{l_1+l_2+j}\mathcal{W}_{l_2,l_1,j}(\theta_1,\theta_2,\phi), \quad (14)$$

with $l_1+l_2+j=J=0$. Thus, under permutation of the two He atoms, the wave packet of Eq. (11) remains invariant.

By introducing the expansion of Eq. (11) in Eq. (10) a set of time-dependent coupled equations is obtained

$$i\hbar\frac{\partial C_{v',l_1',l_2',j'}(R_1,R_2,t)}{\partial t} = \sum_{v,l_1,l_2,j}\left[\frac{2(1+\delta_{l_1'l_2'})}{2(1+\delta_{l_1l_2})}\right]^{1/2}[\langle\chi_{v'}(r)\mathcal{W}_{l_1',l_2',j'}(\theta_1,\theta_2,\phi) \times|\hat{H}|\chi_v(r)\mathcal{W}_{l_1,l_2,j}(\theta_1,\theta_2,\phi)\rangle C_{v,l_1,l_2,j}(R_1,R_2,t) +\langle\chi_{v'}(r)\mathcal{W}_{l_1',l_2',j'}(\theta_1,\theta_2,\phi)|\hat{H}|\chi_v(r)\mathcal{W}_{l_2,l_1,j} \times(\theta_1,\theta_2,\phi)\rangle C_{v,l_2,l_1,j}(R_1,R_2,t)]e^{i(E_{v'}-E_v)t/\hbar}, \quad (15a)$$

and similarly,

$$i\hbar\frac{\partial C_{v',l_2',l_1',j'}(R_1,R_2,t)}{\partial t} = \sum_{v,l_1,l_2,j}\left[\frac{2(1+\delta_{l_1'l_2'})}{2(1+\delta_{l_1l_2})}\right]^{1/2}[\langle\chi_{v'}(r)\mathcal{W}_{l_2',l_1',j'}(\theta_1,\theta_2,\phi) \times|\hat{H}|\chi_v(r)\mathcal{W}_{l_1,l_2,j}(\theta_1,\theta_2,\phi)\rangle C_{v,l_1,l_2,j}(R_1,R_2,t) +\langle\chi_{v'}(r)\mathcal{W}_{l_2',l_1',j'}(\theta_1,\theta_2,\phi)|\hat{H}|\chi_v(r)\mathcal{W}_{l_2,l_1,j} \times(\theta_1,\theta_2,\phi)\rangle C_{v,l_2,l_1,j}(R_1,R_2,t)]e^{i(E_{v'}-E_v)t/\hbar}. \quad (15b)$$

By expanding the angular dependence of the $Cl_2(B)-He_2$ potential in spherical harmonics, the angular quadratures involved in the calculation of the Hamiltonian matrix elements of Eqs. (15) can be evaluated analytically. Expressions for these matrix elements have been given elsewhere.[43]

D. Numerical details

In order to reduce the computational requirements of the present problem one can take advantage of some features of the system. One of them is the high symmetry of Cl_2-He_2. Because of the symmetry property reflected in Eq. (13), solution of only one of the two Eqs. (15) [e.g., Eq. (15a)] is required. Symmetry also helps to save CPU time in the evaluation of the action of some Hamiltonian terms on the wave packet. In addition, the representation of the Hamiltonian in the angular basis set leads to sparse Hamiltonian matrices. By identifying and handling only the nonzero matrix elements substantial savings in memory and CPU time are achieved. Despite the above reductions, the present dynamical computations are still very demanding. Therefore, a compromise has to be achieved between keeping the problem tractable and obtaining a reasonable convergence which allows for a meaningful comparison with experimental data.

The $C_{v,l_1,l_2,j}(R_1,R_2,t)$ packets are represented on a uniform grid in the R_1 and R_2 coordinates, with $R_0=3.0$ a.u., $\Delta R=0.45$ a.u., and $N_R=70$ points. In the basis set four vibrational states $\chi_v(r)$, with $v=v'$, $v'-1$, $v'-2$, and $v'-3$ are included. All the Hamiltonian operations on $C_{v,l_1,l_2,j}(R_1,R_2,t)$ involving kinetic-energy terms are performed using fast Fourier transform (FFT) techniques. The size of the angular basis set is $l_1^{\max}=l_2^{\max}=14$ and $j^{\max}=18$. Since Cl_2 is homonuclear the even and odd j states do not mix, and only the even states have been included in the basis set. These values lead to 569 angular basis functions with $J=0$, out of which 105 correspond to $l_1=l_2$ and 464 to $l_1\neq l_2$ (half of them being $\mathcal{W}_{l_1,l_2,j}$ and the other half being $\mathcal{W}_{l_2,l_1,j}$ functions). The time propagation of the $C_{v,l_1,l_2,j}(R_1,R_2,t)$ packets is carried out by means of the symmetric finite differencing method,[18] up to a final time $t_f=5$ ps with a time step $\Delta t=0.001\,15$ ps.

The wave packet is absorbed before reaching the edges of the grid in the R_1 and R_2 coordinates. Absorption is carried out after each time step Δt by multiplying each packet $C_{v,l_1,l_2,j}(R_1,R_2,t)$ by a product of exponential functions in

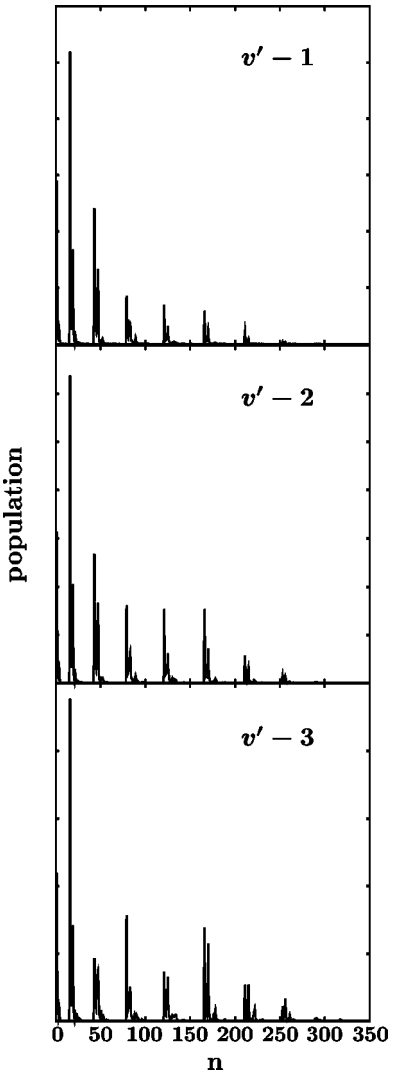

FIG. 1. Population of the angular basis functions at the end of the wave packet propagation ($t_f=5$ ps) in the three $v'-1$, $v'-2$, and $v'-3$ dissociation channels for the $v'=10$ case, vs n, an ordering number for the angular functions. See the text for details.

R_1 and R_2, as previously described.[35,36] The parameters of the absorption exponential functions are $\alpha=0.3$ a.u.$^{-2}$ and $R_{abs}=27.0$ a.u. For the analysis of product distributions the vdW bonds are considered effectively broken for distances $R_1, R_2 > R_c = 16.5$ a.u.

Several convergence tests were carried out. By decreasing the ΔR grid spacing no significant changes were found. Convergence with respect to the angular basis functions was also checked. Figure 1 shows the population $\langle C_{v,l_1,l_2,j}|C_{v,l_1,l_2,j}\rangle$ (or $\langle C_{v,l_2,l_1,j}|C_{v,l_2,l_1,j}\rangle$) of the angular functions at $t=t_f$ for predissociation of the initial state $Cl_2(B,v'=10)-He_2$ through the three vibrational channels $v'-1$, $v'-2$, and $v'-3$. Among the initial states studied, $v'=10$ is that for which the energy available for the vdW modes is largest. Population is shown versus n, an ordering number for the angular functions. The populations corresponding to the $\mathcal{W}_{l_1,l_2,j}$ and $\mathcal{W}_{l_2,l_1,j}$ functions (when $l_1 \neq l_2$) have been added together, and this is why n goes up to 337. The population appears in bands or groups of peaks, each band including all the l_1, l_2 combinations associated with a given j value which lead to $J=0$. For increasing n the ordering of the j bands is $j=0,2,\ldots,18$. The figure shows that the population of each j band decays to zero, meaning that convergence is achieved with the l_1^{max} and l_2^{max} values used. As n increases the population of the j bands decays to zero as well, implying that $j^{max}=18$ suffices for convergence. Similar plots to those of Fig. 1 for $t=t_f$ were found at intermediate times in the wave packet propagation, and this holds also for the $v'>10$ initial states studied.

III. RESULTS AND DISCUSSION

A. Resonance decay lifetimes

The observables of dynamical interest in the VP process of $Cl_2(B)-He_2$ are typically the resonance decay lifetime, and the vibrational and rotational distributions of the Cl_2 fragment. Resonance lifetimes τ can be obtained by fitting the square of the wave packet autocorrelation function $|C(t)|^2=|\langle\psi(0)|\psi(t)\rangle|^2$ to an exponential law of decay, $|C(t)|^2 \simeq e^{-t/\tau}$, and from τ the resonance linewidth Γ can be extracted as $\Gamma=\hbar/\tau$. The single exponential decay assumed implies that the initial state is a pure, isolated resonance, which is essentially our case.

It has been shown[46] that by propagating the wave packet until a time t_f one can obtain $C(t)$ until a time $2t_f$, which in this work is 10 ps. Details of the calculation of the autocorrelation function when the wave packet is absorbed have been given elsewhere.[36] The decay curves $|C(t)|^2$ and their corresponding exponential fits are shown in Fig. 2 for the initial vibrational states v' studied. Lifetimes and linewidths extracted from those fits are listed in Table II, along with the experimental ones. Calculated and experimental lifetimes of the $Cl_2(B,v')-He$ complex, τ_{tri}^{calc} and τ_{tri}^{exp}, respectively, as well as $\tau_{tri}^{calc}/2$ and $\tau_{tri}^{exp}/2$, are also shown for comparison.

The calculated resonance linewidths agree with the measured ones typically within the experimental error. Only in the case of $v'=13$ the calculated linewidth is outside the error limits. The result for $v'=13$ is not surprising, since the $Cl_2(B)-He$ potential surface was fitted to experimental data in the range $v'=8-12$ of Cl_2 vibrational states.[22] As discussed in that work, it is expected that the potential will gradually deteriorate outside that range. The good agreement between the calculated and experimental linewidths of Table II indicates that the $Cl_2(B)-He_2$ potential used here is reasonably accurate, at least for the vibrational states v' investigated. The present results are encouraging since experimental VP lifetimes (or linewidths) of $Cl_2(B)-He$ have been traditionally difficult to reproduce with available potential surfaces, and a similar situation is expected for $Cl_2(B)-He_2$.

Due to the weak He–He interaction, the two vdW bonds are expected to be rather weakly coupled. Then dissociation of the two vdW bonds is expected to occur rather independently on each other, following a sequential mechanism in which one bond dissociates first, then the other one. For a dominantly sequential mechanism the $Cl_2(B)-He_2$ linewidth Γ would be $\Gamma \simeq 2\Gamma_{tri}$ (or $\tau \simeq \tau_{tri}/2$).

The experimental $Cl_2(B)-He_2$ lifetimes found for $v'=12,13$ are slightly smaller but very close to $\tau_{tri}^{exp}/2$, while as

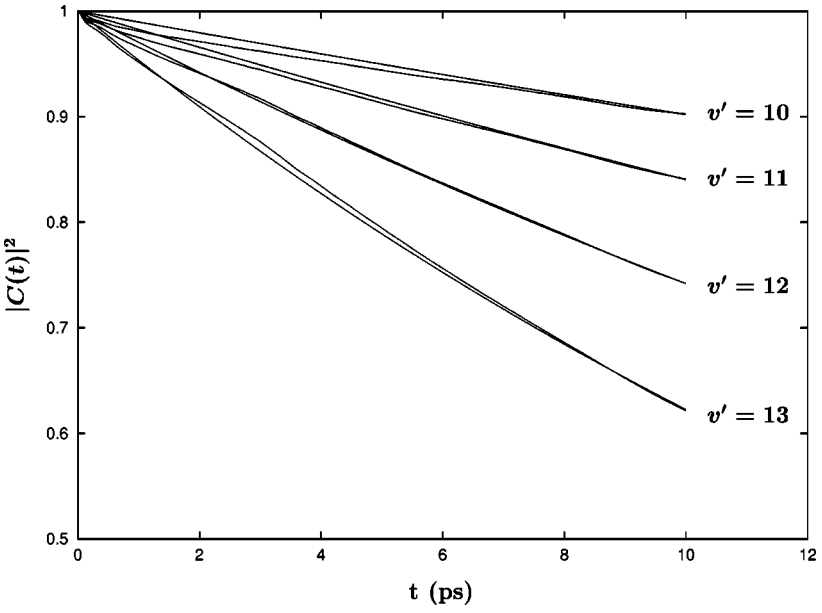

FIG. 2. Decay curves obtained from the wave packet autocorrelation function $C(t)$ for the initial $Cl_2(B,v')$–He_2 resonance states studied vs time. Exponential fits to the curves are also shown.

v' decreases τ^{exp} becomes increasingly smaller than $\tau_{tri}^{exp}/2$ (particularly for $v'=10$). The authors of Ref. 41 suggested some possibilities to explain the differences, such as occurrence of direct $\Delta v'=-1$ dissociation of both He atoms in addition to the sequential one, and acceleration of the first He departure in the sequential process via couplings with the other He atom. It was also pointed out that the differences were within experimental error. The τ^{calc} lifetimes are somewhat smaller than $\tau_{tri}^{calc}/2$, in agreement with the experimental trend, but all of them are close to $\tau_{tri}^{calc}/2$. Thus the present results seem to indicate that the differences between τ^{exp} and $\tau_{tri}^{exp}/2$ for $v'=10,11$ are probably due to the experimental error in the measured linewidth, which is constant for all the v' states ($0.05\ cm^{-1}$), but proportionally increasing with decreasing v'. The calculated $Cl_2(B)-He_2$ lifetimes are consistent with a dominant sequential mechanism of dissociation.

TABLE II. Calculated and experimental linewidths and lifetimes for predissociation of $Cl_2(B,v')-He_2$. The calculated and experimental $Cl_2(B,v')-He$ lifetimes and the corresponding $\tau/2$ values are also shown for comparison.

	$v'=10$	$v'=11$	$v'=12$	$v'=13$
Γ^{calc} (cm^{-1})	0.055	0.092	0.159	0.252
Γ^{exp} (cm^{-1})[a]	0.10 ± 0.05	0.13 ± 0.05	0.21 ± 0.05	0.48 ± 0.05
τ^{calc} (ps)	97.0	57.5	33.5	21.1
τ^{exp} (ps)[b]	53.1	40.8	25.3	11.1
τ_{tri}^{calc} [c]	192	122	78	50
τ_{tri}^{exp} (ps)[d]	179	97	52	25
$\tau_{tri}^{calc}/2$ (ps)	96	61	39	25
$\tau_{tri}^{exp}/2$ (ps)	89.5	48.5	26	12.5

[a]Reference 41.
[b]Obtained from the linewidths of Ref. 41.
[c]Reference 22. The $v'=13$ lifetime has been calculated in this work.
[d]References 1 and 41.

B. Vibrational distributions of Cl_2

Vibrational distributions of the $Cl_2(B,v_f)$ fragment ($v_f=v'-1$, $v'-2$, and $v'-3$) are calculated as described in Ref. 36. In brief, by accumulating probability in the region of the $Cl_2(B,v_f)+He+He$ products, R_1, $R_2>R_c$ (including the absorption region), the probability $P_{v_f}(t)$ of the v_f vibrational channel is calculated along time. Then relative or normalized probabilities are defined as

$$P_{v_f}^{norm}(t)=\frac{P_{v_f}(t)}{\Sigma_v P_v(t)}. \tag{16}$$

The time evolution of the normalized vibrational probabilities $P_{v_f}^{norm}(t)$ is shown in Fig. 3 for the resonance states studied. At short times the probabilities oscillate because the different dissociation channels incorporate with different time scales. Then the probabilities gradually stabilize and converge to a fixed value which gives an estimate of the final vibrational population. After a propagation of 5 ps the probabilities show a reasonably stable behavior in general. In the case $v'=10$, where the VP lifetime is longer, the $v'-1$ and $v'-2$ probabilities are less stable, although no large changes are expected for further times. Table III displays the vibrational populations at final time t_f.

Experimental vibrational populations of the Cl_2 fragment have been reported[26] for predissociation of $Cl_2(B,v'=8)-He_2$. The populations found were 8%, 92%, and less than 1% for the vibrational channels $\Delta v'=-1$, $\Delta v'=-2$, and $\Delta v'=-3$, respectively. The dominant $\Delta v'=-2$ channel is consistent with a sequential mechanism dominating the predissociation process. In contrast to the experimental result for $v'=8$, the present calculations predict very high populations for the $\Delta v'=-1$ dissociation channel, which becomes even dominant for $v'=10$. The expected trend is that the $v'-1$ population will decrease with increasing v', as found in the results of Table III. Thus, based on the experimental

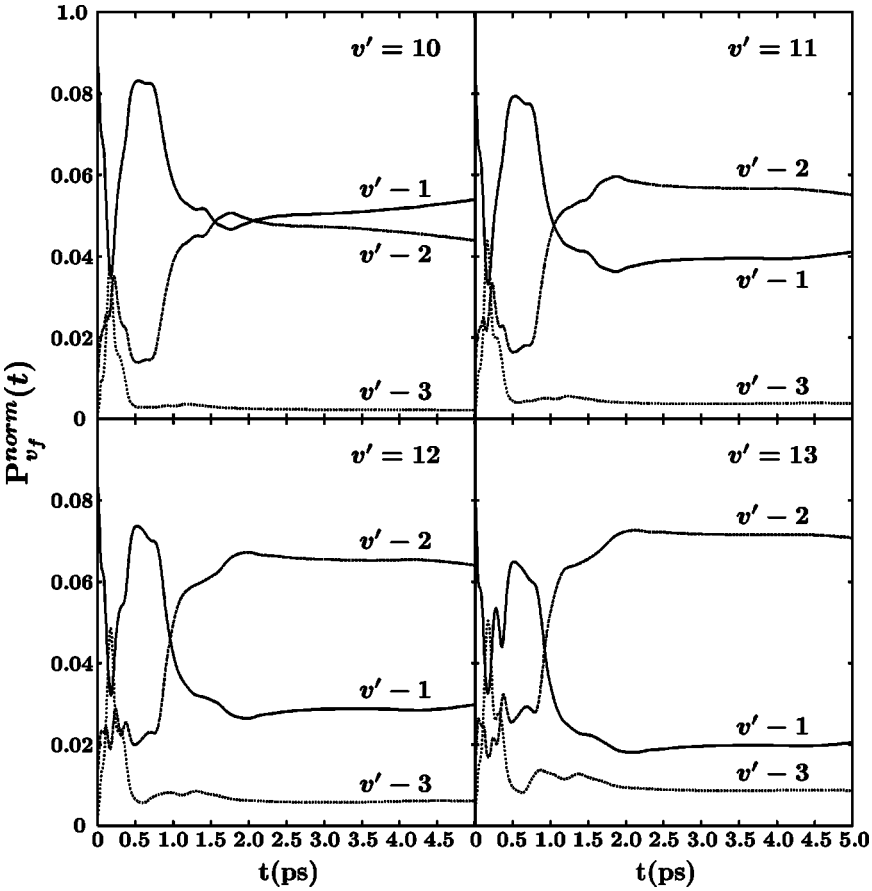

FIG. 3. Time evolution of the normalized vibrational populations of the $Cl_2(B,v_f)$ fragment ($v_f=v'-1$, $v'-2$, $v'-3$) for the initial Cl_2 vibrational excitations v' studied. See the text for details.

data, the $v'-1$ populations in the range $v'=10-13$ are expected to be smaller than 8%, in clear disagreement with the calculated result. In addition, the result of lifetimes consistent with a dominant sequential mechanism through the $\Delta v'=-2$ channel on the one side, and such a high $v'-1$ populations (particularly for $v'=10,11$) on the other side, appears surprising in principle.

The origin of the discrepancy is an artifact in the calculation of the vibrational populations due to the absorption of the wave packet, which causes the $v_f=v'-1$ population to be overestimated at the expense of the $v'-2$ and $v'-3$ populations.[35,36,39] Indeed, after Cl_2 loses one vibrational quantum, some $Cl_2(B,v'-1)-He+He$ wave packet components are absorbed before further dissociation through the $\Delta v'=-2$ and $\Delta v'=-3$ channels occurs (which implies a longer time scale). This leads to underestimate the $v_f<v'-1$ populations, and therefore to overestimate the $v_f=v'-1$ population. This effect can be minimized only by using large grids and placing the absorption region as far as possible in the asymptotic region.[39] Unfortunately, this becomes extremely costly with the present computational means. The implication is that with the present grid limitations it is not possible to calculate quantitatively reliable vibrational populations. In the light that the calculated $v'-1$ populations should be smaller in the absence of the artifact, the apparent inconsistency between the lifetimes obtained and the high $v'-1$ populations disappears.

TABLE III. Calculated $Cl_2(B,v_f)$ fragment vibrational populations (in percentage) after predissociation through the channels $v_f=v'-1$, $v'-2$, and $v'-3$.

v'	$v'-1$	$v'-2$	$v'-3$
10	53.9	43.9	0.2
11	41.1	55.0	3.9
12	29.8	64.0	6.2
13	20.5	70.8	8.7

The 8% of $v'-1$ population found experimentally for $v'=8$ is a remarkable one, and it is interesting to analyze the dissociation mechanisms involved in this channel. The calculated lifetimes along with the qualitative trend found for the vibrational populations can provide some insight on such mechanisms. Two possible mechanisms are direct predissociation to $Cl_2(B,v_f=v'-1)+2He$ or predissociation mediated by redistribution of energy between the two vdW bonds. It is likely that the two mechanisms occur, the question being whether one of them is dominant.

Direct predissociation via the $\Delta v'=-1$ channel is expected to be faster (by about a factor of 2) than sequential dissociation through the $\Delta v'=-2$ channel. The direct mechanism would lead to lifetimes τ^{calc} appreciably shorter than $\tau_{tri}^{calc}/2$, and this effect should be more pronounced as the $v'-1$ population increases. However, the opposite result is found, with $\tau^{calc}\simeq\tau_{tri}^{calc}/2$ for $v'=10,11$, where the $v'-1$ populations are highest, while τ^{calc} becomes increasingly shorter with respect to $\tau_{tri}^{calc}/2$ for $v'=12,13$. This result seems to indicate an important weight of the energy redistribution mechanism. Energy redistribution between the vdW

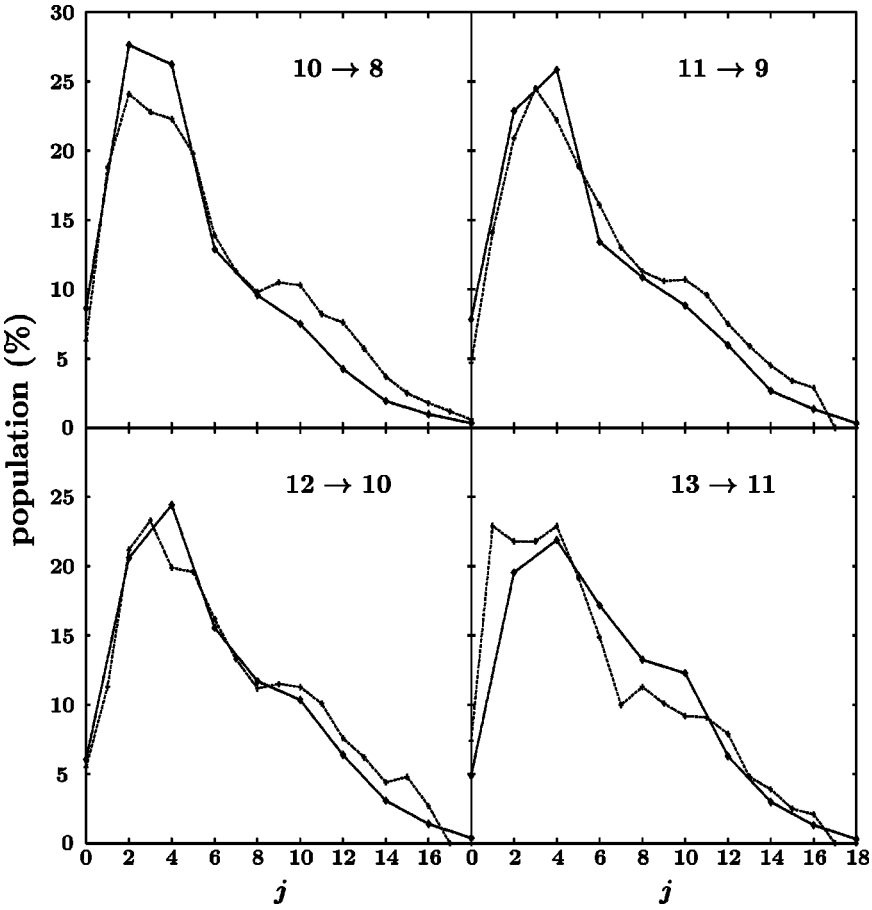

FIG. 4. Calculated (solid line) and experimental (dashed line) $Cl_2(B,v_f,j)$ fragment rotational distributions after vibrational predissociation of $Cl_2(B,v')$–He_2 through the $v_f=v'-2$ channel. The label in each plot stands for $v'\rightarrow v_f$.

modes takes some time to occur, and this additional time would roughly compensate the shorter time it takes losing a single vibrational quantum compared to losing two quanta, in the case of the lower $v'=10,11$ states. The proportionally increasing deviation of τ^{calc} from $\tau^{\mathrm{calc}}_{\mathrm{tri}}/2$ as v' increases ($v'=12,13$) would be consistent with an increasing strength of the vdW intermode couplings, leading to a more efficient (faster) energy redistribution. The implication is that, despite the weak He–He interaction, the couplings between the vdW modes are able to redistribute energy rather efficiently.

C. Rotational distributions of Cl_2

Rotational distributions of the $Cl_2(B,v_f,j)$ fragment have been calculated by projecting out the asymptotic wave packet (i.e., for $R_c<R_1$ $R_2<R_{\mathrm{abs}}$) at $t=t_f$ onto the $Cl_2(B,v_f,j)+He+He$ product states. The distributions (for even j) corresponding to the $v_f=v'-2$ and $v'-1$ predissociation channels are displayed in Figs. 4 and 5, respectively, for all the resonance states investigated. It is noted that the calculated rotational distributions are not significantly affected by the artifact in the calculation of the vibrational populations. If the absorbed $Cl_2(B,v'-1)-He+He$ wave packet components were allowed to dissociate into $Cl_2(B,v'-2)+He+He$, their contribution to the $v'-2$ rotational distribution would be similar as that of the components which actually dissociated before being absorbed.

The $v'-2$ distributions are in very good agreement with those measured experimentally[26] (also shown in Fig. 4). The calculated distributions reproduce well the positions of the maxima of the even j experimental distributions, which are $j=2$, $j=4$, $j=2$, and $j=4$ for $v'=10$, $v'=11$, $v'=12$, and $v'=13$, respectively.[26] The only exception is $v'=12$ for which the maximum of the present distribution occurs at $j=4$ instead of at $j=2$. In general, the distributions underestimate rotational excitation to some extent, and they exhibit a somewhat higher population than the measured one for low j states. In this sense, the slight bimodality found experimentally as a second maximum around $j=10$ is not completely reproduced. It is noted, however, that the distributions exhibit a weak shoulder around $j=10$ (more pronounced for $v'=12,13$), indicating that the bimodality is also predicted by the theoretical distributions, albeit more weakly than in the experimental data. A slight heating of the distributions is found with increasing v', meaning that the present potential describes better rotational excitation for higher v' in the present range of vibrational excitations. In agreement with the experimental finding, the four distributions are quite similar, therefore being rather independent of the initial v' state and of the amount of kinetic energy available for products.

For the $v'-1$ dissociation channel no experimental rotational distributions were reported. As in the case of the $v'-2$ distributions, the $v'-1$ ones are rather independent of the initial v' state excited and of the kinetic energy available for the products. Interestingly, the distributions of Fig. 5 are remarkably more excited than the $v'-2$ ones, displaying a

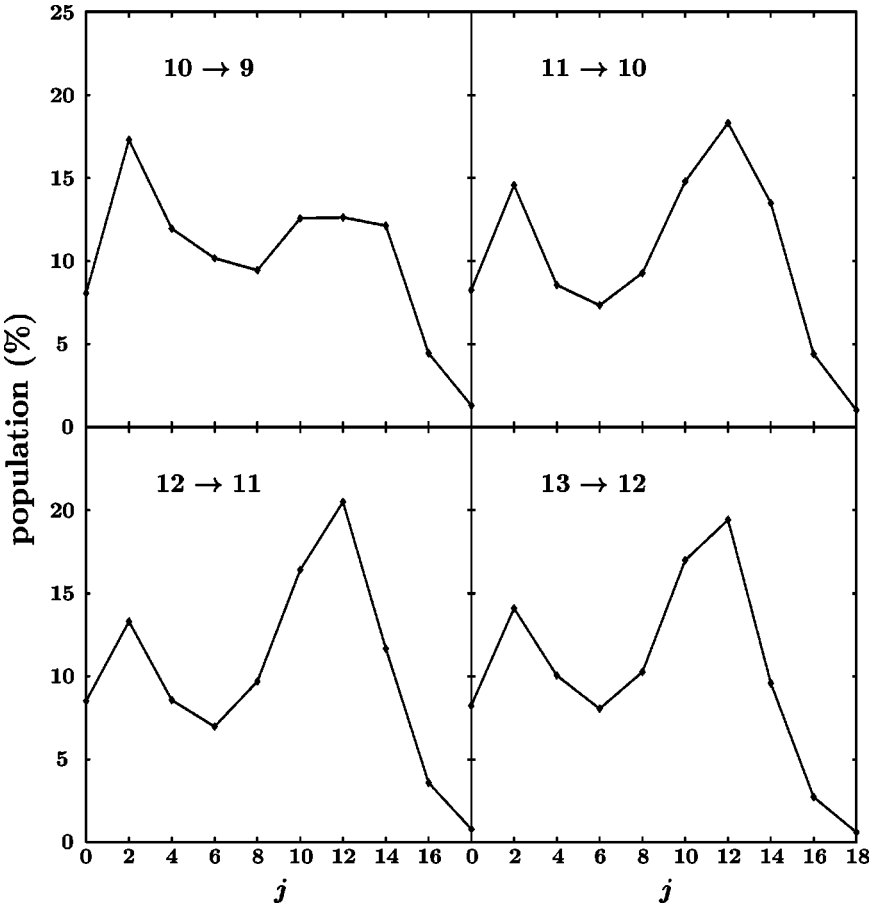

FIG. 5. Same as Fig. 4 but for the calculated rotational distributions after predissociation through the $v_f=v'-1$ vibrational channel.

clear bimodality with two peaks, and with the absolute maximum corresponding typically to the second peak at $j=12$. This behavior contrasts with the Cl_2 rotational distributions obtained after predissociation of $Cl_2(B)-Ne_2$, where the $v'-1$ distributions are colder than the $v'-2$ ones.[34] The higher excitation of the present $v'-1$ distributions cannot be attributed to the kinetic energy available for rotation since, on the one side, this energy is smaller for the $v'-1$ channel than for the $v'-2$ one, and on the other side, the distributions appear to be very independent on the kinetic energy available. The different $v'-1$ and $v'-2$ rotational distributions would indicate that different dissociation mechanisms occur in the two vibrational channels. Again, a mechanism of energy redistribution in the $v'-1$ case, channeling part of the first Cl_2 quantum of vibrational energy to the rotational modes, is consistent with the higher rotational excitation of the $v'-1$ distributions.

IV. CONCLUSIONS

The $Cl_2(B,v')-He_2$ vibrational predissociation dynamics is investigated by applying a full-dimensional, fully coupled wave packet method (assuming $J=0$). The dynamics is simulated for resonance states of the complex corresponding to four initial vibrational excitations $v'=10-13$, and the results are compared with available experimental data. Good agreement is found for the resonance lifetimes (reproduced typically within experimental error) and the Cl_2 fragment rotational distributions. The results show that dissociation is dominantly sequential (one He atom dissociates first, then the other one) through the $\Delta v'=-2$ channel. However, the calculated probabilities for the $\Delta v'=-1$ dissociation channel are found to be overestimated, due to an artifact introduced by the absorption of the wave packet and finite grid limitations. A mechanism of energy redistribution through the couplings between the vdW modes of the two weak bonds is suggested to occur in the dissociation via the $\Delta v'=-1$ channel. Such a mechanism is consistent with the resonance lifetimes obtained, and with the $Cl_2(B,v_f=v'-1)$ rotational distributions predicted, which are remarkably more excited than the $Cl_2(B,v_f=v'-2)$ distributions.

The agreement found with experimental data indicates that the potential surface used to model $Cl_2(B)-He_2$ is reliable enough, at least in the present range of Cl_2 vibrational excitations. This potential is based on a recently reported potential surface for the triatomic $Cl_2(B)-He$ complex, and the present results provide an additional test for that surface. In addition to the quality of the potential used, the quantum dynamical method applied allows one to carry out a realistic simulation of the $Cl_2(B)-He_2$ predissociation dynamics.

ACKNOWLEDGMENTS

The author wishes to thank Professor K. C. Janda for making available the experimental Cl_2 rotational distributions. This work was supported by C.I.C.Y.T. (Ministerio de Ciencia y Tegnología), Spain, Grant No. BFM-2001-2179, and by the European network TMR Grant No. HPRN-CT-

1999-00005. The Centro de Supercomputación de Galicia (CESGA) is acknowledged for allocation of computer time.

[1] J. I. Cline, D. D. Evard, F. Thommen, and K. C. Janda, J. Chem. Phys. **84**, 1165 (1985); J. Williams, A. Rohrbacher, and J. Seong *et al.*, *ibid.* **111**, 997 (1999).
[2] J. I. Cline, N. Sivakumar, D. D. Evard, C. R. Bieler, B. P. Reid, N. Halberstadt, S. R. Hair, and K. C. Janda, J. Chem. Phys. **90**, 2605 (1989).
[3] D. D. Evard, C. R. Bieler, J. I. Cline, N. Sivakumar, and K. C. Janda, J. Chem. Phys. **89**, 2829 (1988).
[4] L. J. van de Burgt, J.-P. Nicolai, and M. C. Heaven, J. Chem. Phys. **81**, 5514 (1984).
[5] D. G. Jahn, S. G. Clement, and K. C. Janda, J. Chem. Phys. **101**, 283 (1994).
[6] A. Rohrbacher, T. Ruchti, K. C. Janda, A. A. Buchachenko, M. I. Hernández, T. González-Lezana, P. Villarreal, and G. Delgado-Barrio, J. Chem. Phys. **110**, 256 (1999).
[7] N. Sivakumar, J. I. Cline, C. R. Bieler, and K. C. Janda, Chem. Phys. Lett. **147**, 561 (1988).
[8] M. Nejad-Sattari and T. A. Stephenson, J. Chem. Phys. **106**, 5454 (1997).
[9] W. Sharfin, K. E. Johnson, L. Warton, and D. H. Levy, J. Chem. Phys. **71**, 1292 (1979).
[10] J. E. Kenny, K. E. Johnson, W. Sharfin, and D. H. Levy, J. Chem. Phys. **72**, 1109 (1980).
[11] M. Gutmann, D. M. Willberg, and A. H. Zewail, J. Chem. Phys. **97**, 8037 (1992).
[12] D. M. Willberg, M. Gutmann, J. J. Breen, and A. H. Zewail, J. Chem. Phys. **96**, 198 (1992).
[13] A. Burroughs and M. C. Heaven, J. Chem. Phys. **114**, 7027 (2001).
[14] A. Burroughs, G. Kerenskaya, and M. C. Heaven, J. Chem. Phys. **115**, 784 (2001).
[15] J. M. Skene and M. I. Lester, Chem. Phys. Lett. **116**, 93 (1985).
[16] J. C. Drobits and M. I. Lester, J. Chem. Phys. **89**, 4716 (1988).
[17] R. L. Waterland, M. I. Lester, and N. Halberstadt, J. Chem. Phys. **92**, 4261 (1990).
[18] S. K. Gray and C. E. Wozny, J. Chem. Phys. **91**, 7671 (1989); **94**, 2817 (1991).
[19] O. Roncero, P. Villarreal, G. Delgado-Barrio, N. Halberstadt, and K. C. Janda, J. Chem. Phys. **99**, 1035 (1993).
[20] T. González-Lezana, M. I. Hernández, G. Delgado-Barrio, A. A. Buchachenko, and P. Villarreal, J. Chem. Phys. **105**, 7454 (1996).
[21] A. García-Vela, J. Phys. Chem. A **106**, 6857 (2002).
[22] A. García-Vela, J. Chem. Phys. **119**, 5583 (2003).
[23] B. A. Swartz, D. E. Brinza, C. M. Western, and K. C. Janda, J. Phys. Chem. **88**, 6272 (1984).
[24] J. C. Drobits and M. I. Lester, J. Chem. Phys. **86**, 1662 (1987).
[25] S. R. Hair, J. I. Cline, C. R. Bieler, and K. C. Janda, J. Chem. Phys. **90**, 2935 (1989).
[26] W. D. Sands, C. R. Bieler, and K. C. Janda, J. Chem. Phys. **95**, 729 (1991).
[27] M. Gutmann, D. M. Willberg, and A. H. Zewail, J. Chem. Phys. **97**, 8048 (1992).
[28] A. García-Vela, P. Villarreal, and G. Delgado-Barrio, J. Chem. Phys. **92**, 6504 (1990).
[29] A. García-Vela, P. Villarreal, and G. Delgado-Barrio, J. Chem. Phys. **94**, 7868 (1991).
[30] A. García-Vela, J. Rubayo-Soneira, G. Delgado-Barrio, and P. Villarreal, J. Chem. Phys. **104**, 8405 (1996).
[31] Z. Li, A. Borrmann, and C. C. Martens, J. Chem. Phys. **97**, 7234 (1992).
[32] M. I. Hernández, A. García-Vela, C. García-Rizo, N. Halberstadt, P. Villarreal, and G. Delgado-Barrio, J. Chem. Phys. **108**, 1989 (1998).
[33] S. F. Alberti, N. Halberstadt, J. A. Beswick, A. Bastida, J. Zúñiga, and A. Requena, J. Chem. Phys. **111**, 239 (1999).
[34] A. Bastida, B. Miguel, J. Zúñiga, A. Requena, N. Halberstadt, and K. C. Janda, J. Chem. Phys. **111**, 4577 (1999).
[35] F. Le Quéré and S. K. Gray, J. Chem. Phys. **98**, 5396 (1993).
[36] M. Ceotto and A. García-Vela, J. Chem. Phys. **115**, 2146 (2001).
[37] O. Roncero, G. Delgado-Barrio, M. I. Hernández, J. Campos-Martínez, and P. Villarreal, Chem. Phys. Lett. **246**, 187 (1995).
[38] J. Campos-Martínez, M. I. Hernández, O. Roncero, P. Villarreal, and G. Delgado-Barrio, Chem. Phys. Lett. **246**, 197 (1995).
[39] A. García-Vela, J. Chem. Phys. **116**, 6595 (2002).
[40] C. Meier and U. Manthe, J. Chem. Phys. **115**, 5477 (2001).
[41] M. I. Hernández, N. Halberstadt, W. D. Sands, and K. C. Janda, J. Chem. Phys. **113**, 7252 (2000).
[42] K. T. Tang and J. P. Toennies, J. Chem. Phys. **118**, 4976 (2003).
[43] P. Villarreal, O. Roncero, and G. Delgado-Barrio, J. Chem. Phys. **101**, 2217 (1994).
[44] R. N. Zare, *Angular Momentum* (Wiley, New York, 1988).
[45] A. R. Edmonds, *Angular Momentum in Quantum Mechanics* (Princeton University, Princeton, 1957).
[46] V. Engel, Chem. Phys. Lett. **189**, 76 (1992).